Ferromagnetic resonance in $Ga_{1-x}Mn_xAs$: Effects of magnetic anisotropy

X. Liu, Y. Sasaki, and J. K. Furdyna*
Department of Physics, University of Notre Dame, Notre Dame, Indiana 46556
(Received 22 November 2002; revised manuscript received 12 March 2003; published 8 May 2003)

This paper describes a systematic study of ferromagnetic resonance (FMR) carried out on a series of specimens of the ferromagnetic semiconductor $Ga_{1-x}Mn_xAs$ in thin film form. The GaMnAs layers were grown by low-temperature molecular beam epitaxy either on GaAs or on GaInAs buffers, the two buffers being used to obtain different strain conditions within the ferromagnetic layer. Our aim has been to map out the dependence of the FMR position on temperature and on the angle between the applied magnetic field and crystallographic axes of the sample. The analysis of the FMR data allowed us to obtain the values of the cubic and the uniaxial magnetic anisotropy fields—i.e., those which are associated with the natural (undistorted) zinc blende structure and those arising from of strain.

DOI: 10.1103/PhysRevB.67.205204 PACS number(s): 75.50.Pp, 76.50.+g, 76.30.−v, 75.70.Ak

I. INTRODUCTION

Ferromagnetic (FM) semiconductors have recently attracted a great deal of attention due to their possible "spintronic" applications.[1–3] Specifically, the development of these materials holds promise of integrating ferromagnetic and nonmagnetic semiconductors, with an eye on developing new devices that depend on electron charge as well as on its spin. Ferromagnetic III-Mn-V alloys are fabricated by low temperature molecular beam epitaxy (LT-MBE), which allows one to achieve much higher degree of Mn solubility in the III-V hosts than is possible at standard temperatures used for growing the host materials. Note that in forming the $Ga_{1-x}Mn_xAs$ alloy, Mn atoms are incorporated at the Ga lattice sites as Mn^{++} ions, thus acting both as magnetic moments and as acceptors.[3] The resulting high concentration of free holes mediates magnetic double-exchange interaction between the Mn^{++} ions, leading to ferromagnetic order consistent with the Zener model proposed by Dietl *et al.*[4] Ferromagnetic order in $Ga_{1-x}Mn_xAs$ is typically observed for $0.02<x<0.08$, with Curie temperatures T_C of 110 K or less for Mn concentrations $x>0.05$ in as-grown specimens.[5] It is now well established that the values of Curie temperature T_C in as-grown GaMnAs can be significantly increased by post-growth annealing at properly chosen annealing temperatures and durations.[6,7]

It has been shown that the magnetic anisotropy of $Ga_{1-x}Mn_xAs$ films is largely controlled by epitaxial strain, with tensile and compressive strain inducing in-plane and out-of-plane moment orientation, respectively.[8] This problem has already been the subject of several theoretical studies.[9] However, despite its importance for a variety of spin-based applications—such as spin-injectors,[10] tunnel junctions,[11] or giant planar Hall effect devices[12]—direct experimental studies of the physics of magnetic anisotropy of $Ga_{1-x}Mn_xAs$ films are still far from complete.

As discussed below, ferromagnetic resonance (FMR) complements the more conventional magnetic studies of FM films by its ability to directly determine magnetic anisotropy parameters,[13] and in this paper we take advantage of the FMR technique to obtain this information on epitaxially grown thin GaMnAs films under various strain conditions. In an earlier paper[14] we reported preliminary FMR results observed on thin GaMnAs films. Here we report a systematic investigation of FMR in GaMnAs films for different Mn concentrations, film thicknesses, strain conditions, and heat treatments. The focus is on the dependence of the FMR field position on temperature and on the angular orientation of the applied magnetic field with respect to the crystal axes, from which we obtain detailed information on magnetic anisotropy fields and on their temperature dependence. As will be seen, the observed anisotropy fields are intrinsically linked to the interplay of the natural GaMnAs zinc blende structure and the effect of strain produced by the lattice mismatch between the GaMnAs film and the underlying substrate.

II. SAMPLE PREPARATION AND EXPERIMENTS

The $Ga_{1-x}Mn_xAs$ samples were grown on (001) semi-insulating "epiready" GaAs substrates in a Riber 32 R&D molecular beam epitaxy (MBE) system. The growth was monitored *in situ* by reflection high energy electron diffraction (RHEED). Standard effusion cells supplied the Ga and Mn fluxes, and the flux of As_2 was produced by a cracker cell. The procedure for MBE growth of the $Ga_{1-x}Mn_xAs$/GaAs was as follows. First a GaAs buffer of thickness 300 nm was grown at a high substrate temperature $T_S\sim590\,°C$ (i.e., under normal GaAs growth conditions). The substrate was then cooled down to 265 °C for low-temperature (LT) growth. Using As_2:Ga beam equivalent pressure ratio of 20:1, a 2-nm-thick buffer layer of LT-GaAs was then grown, followed by a $Ga_{1-x}Mn_xAs$ layer of 100 to 300 nm thickness. For the growth of GaMnAs/GaInAs samples, a GaInAs buffer was first grown at $T_S\sim590°C$ to a thickness of about 1 μm, to allow the GaInAs lattice to relax. The substrate was then cooled as described above, and the GaMnAs layer was finally deposited directly on the GaInAs buffer surface. The RHEED pattern was (1×2) reconstruction during the low-temperature growth of GaMnAs, and no evidence of precipitation of MnAs inclusions (i.e., no spotty RHEED pattern) was observed during the growth. Furthermore, clear RHEED oscillations indicative of two-dimension layer-by-layer growth were observed at the initial stages of GaInAs and GaMnAs deposition. Monitoring the RHEED oscillations provided a precise measure of the

TABLE I. Description of samples used in FMR experiments.

Sample	Buffer	d(nm) [a]	x [b]	T_C(K)	Sample ID
1	GaAs	300	0.03	65	00505H
2	$Ga_{0.85}In_{0.15}As$	300	0.03	50	00315A
3A [c]	GaAs	120	0.08	65	10823C
3B [d]	GaAs	120	0.08	110	10823C
4	GaAs	100	0.08	73	10914A
5	GaAs	200	0.06	65	20327A
6	GaAs	150	0.06	65	20327B
7	GaAs	100	0.06	65	20327C

[a] d: sample thickness.
[b] x: Mn concentration.
[c] As-grown sample.
[d] Sample annealed at 280 °C for 1 h.

growth rate, which allowed us to estimate the In and the Mn concentrations in the deposited layers.

The lattice constants of GaMnAs were measured by x-ray diffraction (XRD) experiments, using a double crystal diffractometer with Cu $K\alpha_1$ radiation. Since the lattice constant of the zinc blende GaMnAs is larger than that of GaAs by an amount that depends on the Mn concentration x, it can be used to determine the concentration x, as follows.[15] Measuring the vertical lattice constants c of the tetragonally distorted layers by XRD allows us to calculate the bulk lattice constants (relaxed values) a_0 of GaMnAs by making two assumptions: that the elastic constants of GaMnAs are equal to those of GaAs and that GaMnAs is coherently strained throughout its thickness by either the underlying GaAs or the GaInAs layer (i.e., $a_{\text{in-plane}}=a_s$ throughout the sample). The Mn concentration x can then be determined from the calculated relaxed lattice constants a_0 using the analysis developed by Schott *et al.* in Ref. 15. Given the assumptions noted above, the values of Mn content determined in this way should be regarded as approximate, with a possible error as high as ± 0.01.

Specifically, we have fabricated seven GaMnAs films for the FMR experiments. The sample parameters of specimens used in this paper are listed in Table I.

As noted above, low-temperature annealing of GaMnAs can dramatically alter the ferromagnetic properties of GaMnAs, most notably by increasing its Curie temperature and changing the temperature dependence of its magnetization to a more mean-field-like behavior.[7] In the context of the present paper, annealing can be used to alter magnetic properties of samples already grown, thus providing the opportunity to compare FMR in GaMnAs films of the same thicknesses but with different magnetic properties. For this purpose, the as-grown samples were cleaved into a number of pieces for systematic annealing. The annealing was carried out in the atmosphere of N_2 gas at the temperature of 280°C. All the samples were annealed at the same fixed flow of N_2 gas equal to 1.5 SCFH (standard cubic feet per h). The time of annealing was 1 h, and the specimens were then cooled by a rapid quench to room temperature under a flow of N_2 gas at 6 SCFH. As expected, magnetization measurements on samples annealed in this manner resulted in an increased T_C and a larger saturation magnetization.

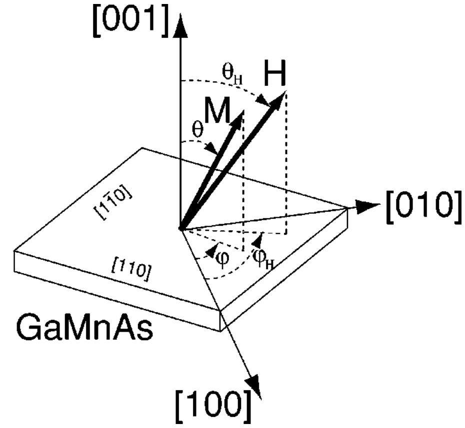

FIG. 1. Coordinate system used in this paper. The orientation of the dc magnetic field H (described by θ_H and φ_H) can be varied continuously in both the $(1\bar{1}0)$ and the (001) planes. The resulting equilibrium orientation of the magnetization M is given by (θ,φ).

The FMR measurements were carried out at 9.46 GHz using an electron paramagnetic resonance (EPR) spectrometer. In this article we will focus on the information obtained from the FMR field position H_R, and on their dependence on temperature and on orientation of the applied dc magnetic field $\mathbf{H}$ relative to the crystal axes of the $Ga_{1-x}Mn_xAs$ specimen. As noted, the GaMnAs films are tetragonally distorted along the growth (i.e., the [001]) direction by either compressive (for GaMnAs/GaAs) or tensile strain (for GaMnAs/GaInAs) in the sample plane. For FMR measurements the samples were cleaved into parallelepipeds with edges along the [110] and $[1\bar{1}0]$ directions, as shown in Fig. 1.

Since the magnetic field of the Bruker EPR system is in the horizontal plane, this allowed two basic geometries for FMR measurements as a function of angular orientation. In the first geometry (subsequently referred to as geometry A) the sample was mounted in the microwave cavity with the layer plane vertical, i.e., with either the [110] or the $[1\bar{1}0]$ direction pointing up. Assuming the $[1\bar{1}0]$ as vertical, this geometry allowed measurement with the dc field $\mathbf{H}$ normal to the layer plane ($\mathbf{H}\|[001]$), in the layer plane ($\mathbf{H}\|[110]$), and in intermediate orientations of the field in the $(1\bar{1}0)$ plane. To discuss the angular dependence of FMR, we define a polar coordinate system shown in Fig. 1. In terms of that system, the field-normal-to-the plane configuration $\mathbf{H}\|[001]$ corresponds to $\theta_H=0°$, and the field-in-the-plane configuration $\mathbf{H}\|[110]$ to $\theta_H=90°$, $\varphi_H=45°$. In the second geometry (geometry B) the sample was mounted with the layer plane horizontal (the [001] direction pointing up). In this geometry we could measure the angular dependence of FMR when the field was confined to the layer [i.e., the (001)] plane, including the orientations $\mathbf{H}\|[110]$ ($\theta_H=90°$, $\varphi_H=45°$), $\mathbf{H}\|[1\bar{1}0]$ ($\theta_H=90°$, $\varphi_H=-45°$) and $\mathbf{H}\|[100]$ ($\theta_H=90°$, $\varphi_H=0°$), as well as intermediate orientations in that plane.

In addition to the FMR measurements as a function of temperature and orientation, systematic dc magnetization measurements were carried out on the samples used in this

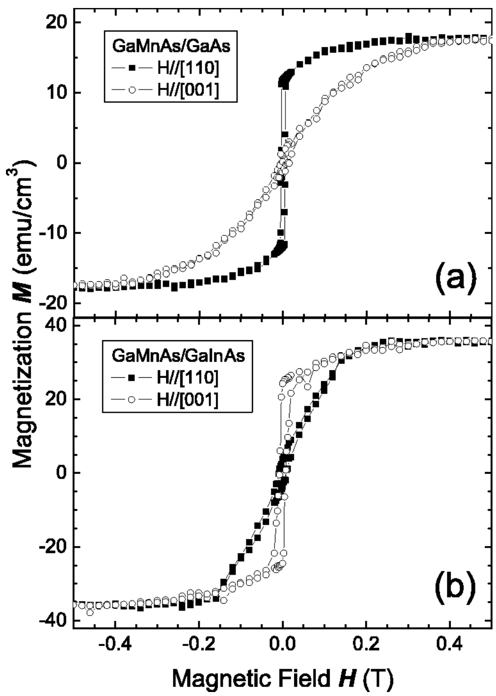

FIG. 2. Magnetization M as function of magnetic field H for a $Ga_{0.97}Mn_{0.03}As$ thin film, measured at $T=5$ K by SQUID for sample No. 1 (top panel) and sample No. 2 (bottom). The magnetic field is applied either in the [110] or in the [001] direction. GaMnAs sample No. 1, grown directly on a (001) GaAs substrate, is under compressive strain in the layer plane; sample No. 2, grown on an $Ga_{0.85}In_{0.15}As$ buffer, is under tensile strain. Note that the easy axis is different for the two samples.

investigation using a commercial superconducting quantum interference device (SQUID) magnetometer. These included the temperature dependence of the magnetization **M**, and hysteresis profiles for **H** applied parallel or normal to the layer plane. Typical hysteresis data are shown in Fig. 2.

The hysteresis profiles in Fig. 2 have special relevance for our analysis of the FMR results, for two reasons. First, these data demonstrate the striking difference in magnetic anisotropy of GaMnAs under compressive (GaMnAs/GaAs, sample No. 1) and tensile strain (GaMnAs/GaInAs, sample No. 2). The hysteresis loops for GaMnAs/GaAs (top panel) clearly shows that the easy axis of magnetization is in the plane of the sample. Qualitatively the behavior seen in the upper panel is typical of GaMnAs/GaAs for all Mn concentrations used in this study (see Table I). In contrast, in the case of the GaMnAs/GaInAs sample, which is under tensile strain, the easy axis is normal to layer plane, as evidenced by the sharp hysteresis loop observed when **H** is applied parallel to the [001] direction (bottom panel).

The second feature of Fig. 2 relevant to this paper involves the hysteresis loops observed when **H** is applied along the hard axes (**H** normal to the plane for GaMnAs/GaAs and **H** in the plane of the film for GaMnAs/GaInAs system, respectively). The feature of interest is that saturation magnetizations coincide for fields of about 0.3 T or less, indicating that fields of that magnitude are sufficient to orient all spins along the hard axis. Since (as will be seen below) FMR with **H** along the hard axis is observed at fields far in excess of 0.3 T, the results shown in Fig. 2 allow us to assume that the magnetization **M** and **H** are collinear ($\theta_H=\theta$; $\varphi_H=\varphi$) for fields applied along that axis, greatly simplifying the analysis of the FMR data.

III. BRIEF THEORETICAL OVERVIEW

In order to interpret the FMR results obtained on the GaMnAs films, we first briefly review the theoretical formulation of FMR, and present expression for the resonance conditions for principal field orientations (e.g., for the dc field **H** applied normal to the sample plane, or in the sample plane along high-symmetry crystalline directions). In this article we use the well-known Landau-Lifshitz-Gilbert equation[13,16] for the precession of the magnetization to describe the dynamics of FMR in a GaMnAs film. In order to determine the magnetic parameters from the data, we start with the expression for the free-energy density F in an applied dc magnetic field H for a zinc blende crystal film (such as GaMnAs) under tetragonal distortion[13]

$$F=-MH[\cos\theta\cos\theta_H+\sin\theta\sin\theta_H\cos(\varphi-\varphi_H)] -2\pi M^2\sin^2\theta-K_{2\perp}\cos^2\theta-\frac{1}{2}K_{4\perp}\cos^4\theta -\frac{1}{2}K_{4\parallel}\frac{1}{4}(3+\cos 4\varphi)\sin^4\theta-K_{2\parallel}\sin^2\theta\sin^2\left(\varphi-\frac{\pi}{4}\right). \tag{1}$$

Here the first term describes the Zeeman energy; the second term is the demagnetizing energy (shape anisotropy); $K_{2\perp}$ and $K_{4\perp}$ are constants representing the perpendicular uniaxial and cubic anisotropy, respectively; the planar anisotropy is given by a uniaxial term $K_{2\parallel}$ and a cubic term $K_{4\parallel}$; and the angles are defined in Fig. 1. The in-plane anisotropy term $K_{2\parallel}$ reflects the fact that in a zinc blende structure the [110] and $[1\bar{1}0]$ directions are not equivalent.[17] Without this term Eq. (1) is the free energy density for an ultrathin film of a purely tetragonal symmetry.[13]

The resonance condition for any given field orientation can be obtained from Eq. (1) in the standard way by minimizing the free energy F with respect to θ and φ.[13,18] We do this for two geometries described below. Using the coordinates defined in Fig. 1, for $\varphi_H=45°$ [**H** and **M** in the $(1\bar{1}0)$ plane, henceforth referred to as geometry A], one finds

$$\left(\frac{\omega}{\gamma}\right)^2=\left[H_R\cos(\theta_H-\theta)+\left(-4\pi M+\frac{2K_{2\perp}}{M}+\frac{K_{4\perp}}{M}-\frac{K_{4\parallel}}{2M}\right)\cos 2\theta+\left(\frac{K_{4\perp}}{M}+\frac{K_{4\parallel}}{2M}\right)\cos 4\theta\right] \times\left[H_R\cos(\theta_H-\theta)+\left(-4\pi M+\frac{2K_{2\perp}}{M}+\frac{K_{4\parallel}}{M}\right)\cos^2\theta +\left(\frac{2K_{4\perp}}{M}+\frac{K_{4\parallel}}{M}\right)\cos^4\theta-\frac{2K_{4\parallel}}{M}-\frac{2K_{2\parallel}}{M}\right] \tag{2a}$$

and for $\theta=\theta_H=90°$ (**M** and **H** parallel to the film plane, geometry B) one obtains

$$\left(\frac{\omega}{\gamma}\right)^2=\left[H_R\cos(\varphi-\varphi_H)+\frac{2K_{4\parallel}}{M}\cos 4\varphi-\frac{2K_{2\parallel}}{M}\cos\left(2\varphi-\frac{\pi}{2}\right)\right]\left[H_R\cos(\varphi-\varphi_H)+4\pi M-\frac{2K_{2\perp}}{M}+\frac{K_{4\parallel}}{2M}(3+\cos 4\varphi)+\frac{2K_{2\parallel}}{M}\sin^2\left(\varphi-\frac{\pi}{4}\right)\right]. \tag{2b}$$

Here ω is the angular frequency of the microwave field and $\gamma=g\mu_B\hbar^{-1}$ is the gyromagnetic ratio (g being the spectroscopic splitting factor, and $\hbar$ the Planck constant). For free electrons $g=2.0023$, yielding $\gamma=1.7588\times10^7$ Hz Oe^{-1}. The quantity $4\pi M$ in Eq. (2) gives the demagnetizing field, where $M=M(T, H)$ is the field- and temperature-dependent magnetization, which can be measured independently, e.g., by SQUID.

The magnetic parameters $2K_{2\parallel}/M$, $2K_{4||}/M$, $2K_{4\perp}/M$, $4\pi M-2K_{2\perp}/M\equiv4\pi M_{\mathrm{eff}}$ and γ (or the g factor) can in principle be determined by fitting Eq. (2) to the experimental data for H_R at different θ_{H} and φ_H. Here we give the resonance conditions for specific high-symmetry configurations obtained from the general solution of the FMR equations given in the Eq. (2). It is important to note that, to obtain these high-symmetry results, we have assumed that the magnetization **M** is aligned with the applied field **H**. While this approximation is quite safe for **H** applied along the easy axes of the GaMnAs films, Fig. 2 shows that—as argued above—the fields at which FMR is observed are also sufficiently high to turn **M** parallel to **H** when the latter is applied parallel to the hard axis. Moreover, with $|K_{2\perp}|\gg|K_{4\perp}|$ and $|K_{4\parallel}|\gg|K_{2\parallel}|$, this assumption is expected to hold for most of our data. Thus we obtain for **M** and **H** parallel to [001], i.e., perpendicular to the film plane ($\theta=\theta_H=0°$)

$$\left(\frac{\omega}{\gamma}\right)^2=\left(H_{R\perp}-4\pi M+\frac{2K_{2\perp}}{M}+\frac{2K_{4\perp}}{M}\right)\left(H_{R\perp}-4\pi M+\frac{2K_{2\perp}}{M}+\frac{2K_{4\perp}}{M}-\frac{2K_{2\parallel}}{M}\right), \tag{3a}$$

for **M** and **H** in the film plane, parallel to [100] ($\theta=\theta_H=90°$, $\varphi=\varphi_H=0°$)

$$\left(\frac{\omega}{\gamma}\right)^2=\left(H_{R\parallel}+\frac{2K_{4\parallel}}{M}\right)\left(H_{R\parallel}+4\pi M-\frac{2K_{2\perp}}{M}+\frac{2K_{4\parallel}}{M}+\frac{K_{2||}}{M}\right), \tag{3b}$$

for **M** and **H** in the film plane, parallel to [110] ($\theta=\theta_H=90°$, $\varphi=\varphi_H=45°$)

$$\left(\frac{\omega}{\gamma}\right)^2=\left(H_{R\parallel}-\frac{2K_{4\parallel}}{M}-\frac{2K_{2\parallel}}{M}\right)\left(H_{R\parallel}+4\pi M-\frac{2K_{2\perp}}{M}+\frac{K_{4||}}{M}\right), \tag{3c}$$

and for **M** and **H** in the film plane, parallel to $[1\bar{1}0]$ ($\theta=\theta_H=90°$, $\varphi=\varphi_H=-45°$)

$$\left(\frac{\omega}{\gamma}\right)^2=\left(H_{R\parallel}-\frac{2K_{4\parallel}}{M}+\frac{2K_{2\parallel}}{M}\right)\left(H_{R\parallel}+4\pi M-\frac{2K_{2\perp}}{M}+\frac{K_{4||}}{M}+\frac{2K_{2\parallel}}{M}\right). \tag{3d}$$

It is instructive to identify the origin of the various anisotropy terms appearing in Eqs. (3a)–(3d). The terms involving $K_{2\perp}$ arise from uniaxial anisotropy of the GaMnAs system produced by the tetragonal distortion of the lattice along the [001] direction. The sign of this contribution will thus be opposite for GaMnAs layers under compressive and under tensile strain in the layer plane, leading—as will be seen—to a drastic difference between the FMR positions observed in GaMnAs grown on GaAs and on GaInAs buffers. The in-plane anisotropy term $K_{4\parallel}$ is the fourth-order anisotropy of the cubic system, essentially distinguishing between the $\langle 100\rangle$ and $\langle 110\rangle$ directions and $K_{2\parallel}$ is a very small term arising from the fact that [110] and $[1\bar{1}0]$ are not exactly equivalent due to the specific bond configuration in the zinc blende structure, so that the (001) plane has also a small but finite uniaxial anisotropy.[19] For completeness we note that in a purely cubic system the terms $K_{4\perp}$ and $K_{4\parallel}$ (sometimes denoted as K_1 in the literature) would be identical, but they can in principle differ in a tetragonally-distorted crystal, such as GaMnAs grown on a mismatched substrate. We will see, however, that in the context of the present FMR experiments we will not be able to extract information on the fourth-order cubic out-of-plane anisotropy term $K_{4\perp}$, since contributions arising from this term always occur side-by-side with (and are therefore masked by) the much larger contributions of $K_{2\perp}$ [see Eq. (1)]. Since the various terms involving $2K_i/M$ in Eq. (3) represent effective fields arising from the various magnetic anisotropy components, in what follows we will refer to $2K_i/M$ as anisotropy fields H_i. Note finally that the terms $4\pi M-2K_{2\perp}/M$ always occur together. For that reason it is customary in calculations to lump $4\pi M-2K_{2\perp}/M$ into a single term $4\pi M_{\mathrm{eff}}$.

IV. EXPERIMENT RESULTS AND DISCUSSION

Figure 3 shows FMR spectra for a representative GaMnAs/GaAs film (sample No. 4) in two configurations: with **H** in the plane of the sample ($\theta_{\mathrm{H}}=90°$, $\varphi_H=45°$, $\mathbf{H}\|[110]$) and with **H** normal to the film ($\theta_{\mathrm{H}}=0°$, $\mathbf{H}\|[001]$). In the latter configuration FMR corresponds to the sharp resonance line at 0.81 T. Note that pronounced shifts of the FMR line are observed to fields above and below the $g=2.00$ ($H=\omega/\gamma$) resonance position for the magnetic field orientations perpendicular and parallel to the plane of the layer, respectively. Taken by itself, this behavior could qualitatively be attributed to the effect of demagnetization field $4\pi M$ alone, as can be seen from the analysis of Eq. (3) when the contributions from magnetic anisotropy terms K_i/M are neglected. However, this conclusion is immediately eliminated by the data in Fig. 4, where FMR spectra for

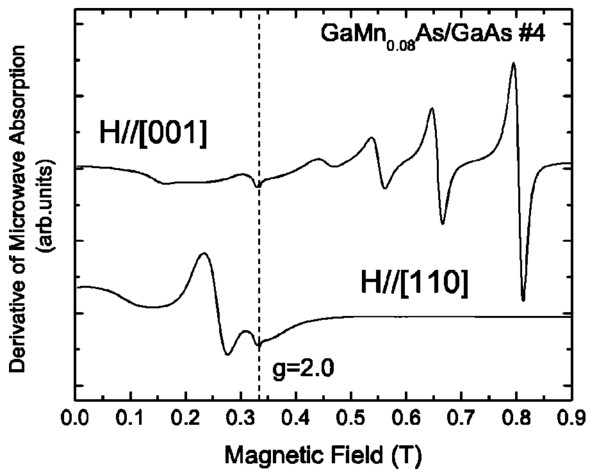

FIG. 3. FMR spectra for parallel ($\mathbf{H}\|[110]$) and perpendicular ($\mathbf{H}\|[001]$) configurations observed for $Ga_{0.92}Mn_{0.08}As/GaAs$ (sample No. 4) at 9.46 GHz and 4.0 K. The resonance position for $g=2.00$ is indicated by the vertical dashed line. For $\mathbf{H}\|[001]$, FMR corresponds to the sharp line at 0.81 T. The series of lines below FMR are spin wave standing wave resonances. The weak resonance at the $g=2.0$ position is ascribed to isolated paramagnetic Mn^{++} ions that may have diffused out of the FM layer.

GaMnAs/GaInAs film (sample No. 2) are also presented for two configurations $\mathbf{H}\|[110]$ and $\mathbf{H}\|[001]$. Specifically, the data show that for tensile strain the FMR shifts *below* the $H=\omega/\gamma$ position for the magnetic field orientation perpendicular to the plane of the layer, and occurs above $H=\omega/\gamma$ for fields applied in the sample plane, contrary to the predictions of Eqs. (3a),(3c) when the anisotropy terms are neglected. The FMR spectra in Figs. 3 and 4 thus establish at the outset that the position of FMR is primarily determined by crystal geometry, i.e., that magnetic anisotropy fields play a dominant role in determining the field at which the resonance occurs. From the data in Figs. 3 and 4 one can immediately infer that the FMR field $H_R>\omega/\gamma$ when $\mathbf{H}$ is parallel to the hard axis.

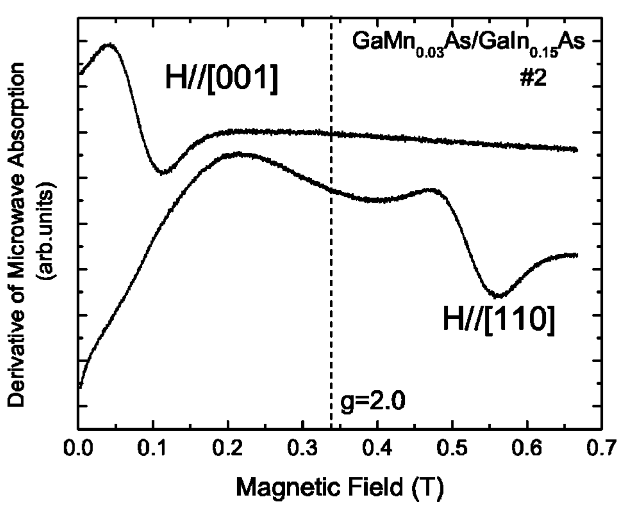

FIG. 4. FMR spectra for parallel ($\mathbf{H}\|[110]$) and perpendicular ($H\|[001]$) configurations observed for $Ga_{0.97}Mn_{0.03}As/Ga_{0.85}In_{0.15}As$ (sample No. 2) at 9.46 GHz and 4.0 K. The resonance position for $g=2.00$ is indicated by the vertical dashed line.

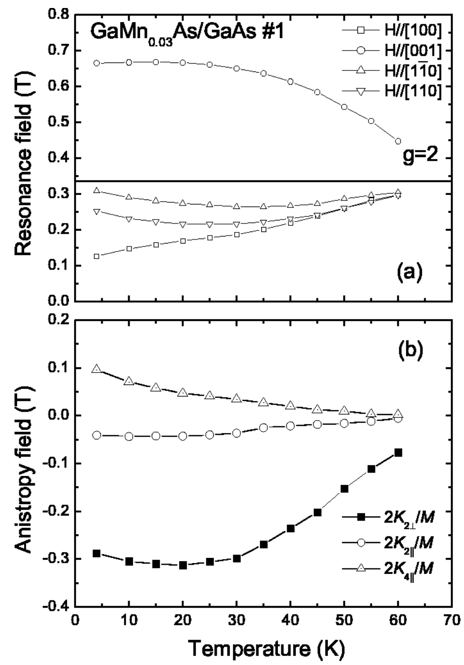

FIG. 5. (a) Temperature dependence of FMR fields observed at four high-symmetry field orientations for $Ga_{0.97}Mn_{0.03}As/GaAs$ (sample No. 1). (b) Magnetic anisotropy fields $2K_{2\perp}/M$, $2K_{2\|}/M$, and $2K_{4\|}/M$ as a function of temperature for the same sample. The solid lines are the guides for the eye.

We note parenthetically that in Fig. 3 the FMR line at 0.81 T is accompanied by a series of spin wave resonances at lower fields. A quantitative discussion of these excitations is beyond the intended scope of the present paper, and will be undertaken in detail at a later time. It is important to point out, however, that—since such resonances represent a Fabry-Perot-like standing wave interference of the magnetization due to spin wave reflections at the sample interfaces—the very presence of spin wave resonances indicates that the magnetic order is coherent (i.e., long range) across the entire sample. Finally, we note in Fig. 3 the presence of a weak line at the $g=2.0$ resonance field. This resonance is probably caused by isolated paramagnetic Mn^{++} ions that may have diffused outside of the FM layer, and is of no interest in the context of this paper.

A. GaMnAs films with compressive strain

Figure 5(a) shows the temperature dependence of the resonance position in four configurations ($\mathbf{H}\|[110]$, $\mathbf{H}\|[1\bar{1}0]$, $\mathbf{H}\|[100]$, and $\mathbf{H}\|[001]$) for the GaMnAs/GaAs film (sample No. 1) corresponding to the top panel of Fig. 2. FMR fields observed for other GaMnAs/GaAs samples listed in Table I show very similar behaviors. As one can see from the figure, the FMR position is strongly shifted to fields above the $g=2.0$ Mn^{++} resonance position ($H=\omega/\gamma$) when the magnetic field is applied perpendicular to the plane of the GaMnAs film, and below the $H=\omega/\gamma$ position when $\mathbf{H}$ is in the plane of the film. These shifts gradually decrease as the

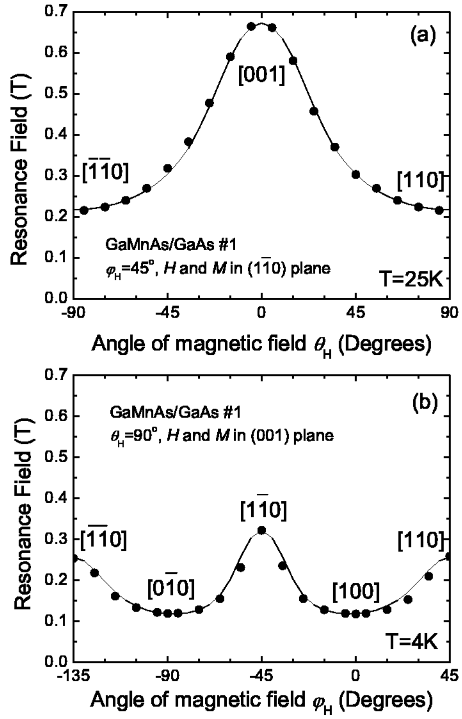

FIG. 6. Angular dependence of FMR fields for $Ga_{0.97}Mn_{0.03}As/GaAs$ (sample No. 1) for (a) magnetic field **H** in the $(1\bar{1}0)$ plane (geometry A); and (b) for **H** in the (001) plane (geometry B). The solid curves in figure represent the positions of H_R calculated theoretically using the full Eqs. (2a) and (2b) for the two geometries, respectively.

temperature increases, the FMR field converging toward $H=\omega/\gamma$ as the Curie temperature is approached.

Using the FMR positions for the four orientations shown in Fig. 5(a) at any one temperature, we can use Eqs. (3a)–(3d) to obtain the value of $4\pi M_{\mathrm{eff}}$, $2K_{4\parallel}/M$, and $2K_{2\parallel}/M$. The bottom panel of Fig. 5 shows the temperature dependence of anisotropy fields $2K_{2\perp}/M=4\pi M-4\pi M_{\mathrm{eff}}$, $2K_{2\parallel}/M$, and $2K_{4\parallel}/M$ for the GaMnAs/GaAs sample corresponding to Fig. 5(a). The values of $M(T)$ used to obtain $2K_{2\perp}/M$ from the calculated value of $4\pi M_{\mathrm{eff}}$ are measured by SQUID. One can see that the magnitudes of all anisotropy fields monotonically decrease when the temperature increases, and approach zero close to the Curie temperature. Note that the GaMnAs/GaAs sample has a negative $2K_{2\perp}/M$, which corresponds to the easy axis of M lying in the plane of the film. This behavior is true of all GaMnAs/GaAs samples listed in Table I.

We have also mapped out the resonance condition for the same GaMnAs/GaAs sample as a function of magnetic field orientation relative to the crystal axes at a fixed temperature. Two geometries were used, as described in Sec. II: geometry A, where we vary θ_H in the $(1\bar{1}0)$ plane, keeping φ_H fixed at 45° (see Fig. 1) and geometry B, where we vary φ_H in the (001) plane while keeping θ_H fixed at 90°. The observed FMR field positions obtained for the two geometries are shown as points in the upper and lower panels of Fig. 6, respectively. Note that the lowest resonance field is observed when **H** lies in the film plane and parallel to the [100] direction ($\theta_{\mathrm{H}}=90°$, $\varphi_H=0°$), as was already seen in Fig. 5(a).

The bottom panel of Fig. 6, which shows the angular dependence of H_R for **H** in the (001) plane, is particularly interesting for two reasons. First, it reveals that magnetic anisotropy (which we attribute to the cubic anisotropy term $H_{4\parallel}$) is quite strong. The origin of this behavior can be ascribed to the anisotropy between the [100] and [110] orientations in the (001) plane, as can be readily seen from the fact that the sign of $H_{4\parallel}$ in the first parenthesis of Eqs. (3b) is opposite from that in Eqs. (3c) and (3d). Second, it is evident from Fig. 6(b) that the symmetry of the FMR position is not exactly fourfold in the (001) plane (as would be expected for a purely tetragonal distortion along the [001] axis), but that a small difference exists between H_R for **H** applied along the [110] and $[1\bar{1}0]$ directions, respectively. This initially unexpected behavior is precisely the consequence of the term $K_{2\parallel}$ in Eqs. (3c) and (3d), which arises from the cation-anion bond topology specific to the (001) zinc blende plane. Similar effects have been seen in α-Fe (bcc) films grown on GaAs, and for a detailed discussion the reader is referred to Ref. 19.

The solid curves in Fig. 6 represent the positions of H_R calculated theoretically using the full Eq. (2). In the calculation we used $g=2.0$ for the Mn^{++} ions and the values of $4\pi M_{\mathrm{eff}}$, $2K_{2\parallel}/M$ and $2K_{4\parallel}/M$ already obtained from the analysis of the high-symmetry orientations via. Eq. (3) (see Fig. 5 and the accompanying discussion). The calculation was carried out by minimizing the free energy with respect to angles φ and θ for any combination of φ_H and θ_H. Since the resonance positions for the different angles represent a set of simultaneous equations, the ability to satisfy the observed data with the same anisotropy parameters is a clear indication that FMR in GaMnAs indeed obeys the model for tetragonal symmetry given by Eq. (1). Specifically, it confirms the values the anisotropy fields obtained using Eq. (3), along with the assumption that **H** and **M** are collinear in the high-symmetry directions. The calculations also reveal, however, that the assumption of collinearity is no longer true for arbitrary directions (it is easy to show that if **H** and **M** were collinear for all angles, the angular variation of H_R would be sinusoidal in Fig. 6). Briefly, the departure from sinusoidal dependence on θ_{H} and φ_H seen in Fig. 6(a) can be understood as follows: once **H** is tilted away from the [001] direction, the orientation of **M** tends to tilt faster than **H** toward the sample plane, seeking the easy axis of magnetization. Using this argument, we can infer from the shape of the angular dependence in Fig. 6(b) that the easy axis is not only confined to the layer plane, but is oriented along the [100] direction, consistent with the conjecture stated earlier that the FMR field H_R has its lowest value when **H** points along the easy axis.

As noted earlier, the FM properties of GaMnAs can be altered (improved) by appropriate annealing.[7] In Fig. 7 we compare the FMR fields for sample No. 3 ($Ga_{0.92}Mn_{0.08}As/GaAs$, very similar to sample No. 4) observed before and after annealing. Note the increase of the resonance shifts observed after heat treatment. The analysis

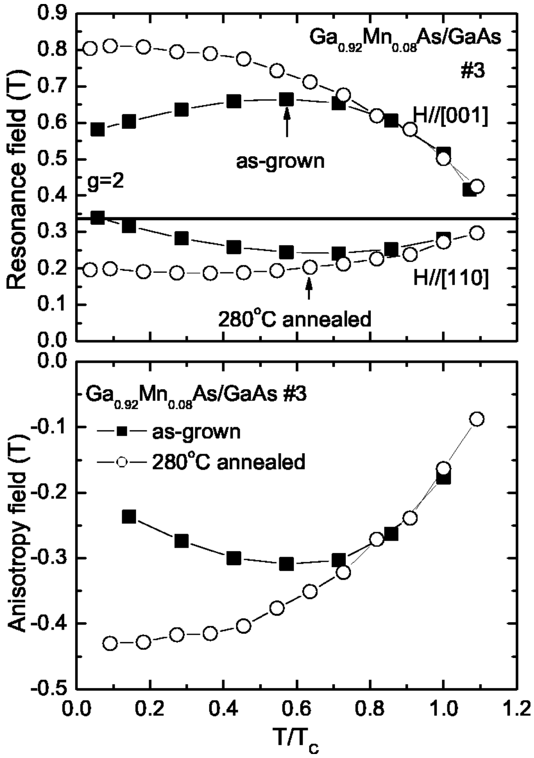

FIG. 7. Top panel: Comparison of temperature dependences of FMR fields observed at two high-symmetry field orientations in the $(1\bar{1}0)$ plane for $Ga_{0.92}Mn_{0.08}As/GaAs$ (sample No. 3) before and after annealing (solid and open symbols, respectively). Bottom panel: Comparison of the anisotropy field $2K_{2\perp}/M$ before and after annealing for the same sample. The solid lines are the guides for the eye.

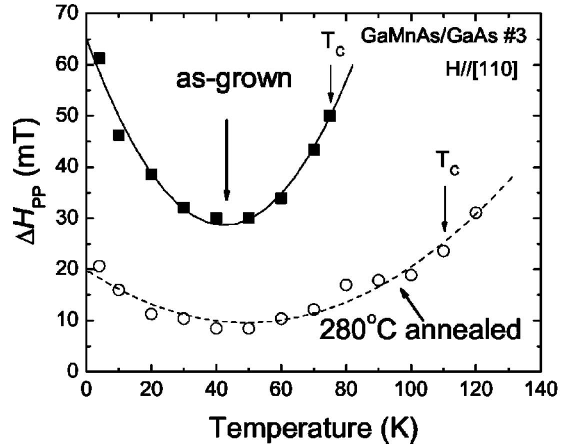

FIG. 8. Comparison of FMR linewidth for $Ga_{0.92}Mn_{0.08}As/GaAs$ (sample No. 3) before and after annealing, observed as a function of temperature in the $\mathbf{H}\|[110]$ orientation. Curie temperatures T_C for the as-grown and annealed cases are also indicated in the figure. The solid and dashed lines are guides for the eye.

of the data indicates that the observed increase is caused primarily by a dramatic increase in the magnitude of $K_{2\perp}$, as seen in the bottom panel of Fig. 7.

We point out parenthetically that the peak-to-peak FMR linewidth ΔH_{pp} observed in our experiments shows a distinct dependence on the orientation of the magnetic field with respect to the crystal axes of the specimen, similar to the angular dependence of the FMR resonance position. Unfortunately the lack of theoretical understanding of FMR broadening mechanisms, such as intrinsic damping and magnetic inhomogeneity within the ferromagnetic film, prevents us from carrying out a meaningful discussion of ΔH_{pp} observed in this set of experiments. Without attempting to analyze ΔH_{pp}, we nevertheless wish to point to the dramatic narrowing of the FMR linewidth observed after GaMnAs has been annealed, as shown in Fig. 8. Since it has already been established that annealing reduces the number of defects (such as Mn interstitials),[20] and since it is reasonable to expect that the annealing process also serves to "smooth out" local inhomogeneities, we are tempted to suggest that the spectacular narrowing of FMR in annealed specimens is in some way related to the overall improvement of materials quality by such post-growth heat treatment.

B. GaMnAs film under tensile strain in the layer plane

We also carried out FMR measurements as function of temperature and angular orientation on a GaMnAs film under tensile strain. As noted earlier, tensile strain was achieved by growing GaMnAs on a relaxed GaInAs buffer, with sufficient In concentration to make the lattice parameter of the buffer larger than that of the FM film. The hysteresis data for the $Ga_{0.97}Mn_{0.03}As/Ga_{0.85}In_{0.15}As$ (sample No. 2 in Table I) are given in the lower panel of Fig. 2, and the FMR spectra are shown in Fig. 4. This situation is interesting because, as Fig. 2 clearly indicates, the tensile strain in the layer plane of the sample causes the easy axis of magnetization to lie perpendicular to the film (i.e., along the [001] direction), contrary to the behavior characterizing most ultrathin FM films, where an in-plane easy axis of M is generally expected owing to the shape anisotropy (demagnetizing) energy. In the context of FMR, the reversal of the sign of the strain leads to a large *positive* $2K_{2\perp}/M$, which counteracts the demagnetization field in Eq. (1), thus shifting the FMR position downward. As already shown in Fig. 4, for the specific value of tensile strain achieved in the present $Ga_{0.97}Mn_{0.03}As/Ga_{0.85}In_{0.15}As$ sample the value of $2K_{2\perp}/M$ is sufficiently large to shift the FMR field *below* the $g=2.0$ position—a feature that alerted us to the dominant role of magnetic anisotropy in determining FMR fields in epitaxially grown GaMnAs.

The top panel of Fig. 9 shows the temperature dependence of the FMR positions observed for the $Ga_{0.97}Mn_{0.03}As/Ga_{0.85}In_{0.15}As$ sample (sample No. 2) in four configurations $\mathbf{H}\|[001]$ and $\mathbf{H}\|[110]$ observed in geometry A and $\mathbf{H}\|[1\bar{1}0]$ and $\mathbf{H}\|[100]$ in geometry B. In contrast to the GaMnAs/GaAs samples, the FMR is now observed at fields *above* the $H=\omega/\gamma$ ($g=2.0$ resonance) position for magnetic field $\mathbf{H}$ parallel to the plane of the film, and below $H=\omega/\gamma$ for the perpendicular geometry. As in the case of the GaMnAs/GaAs FMR data, these shifts decrease rapidly as the Curie temperature is approached, converging on the $g=2.0$ resonance position at higher temperatures. The data collected in Fig. 9(a) corroborate the conjecture made earlier that H_R tends to be shifted above the $g=2.0$ position when field $\mathbf{H}$ is parallel to the hard axis.

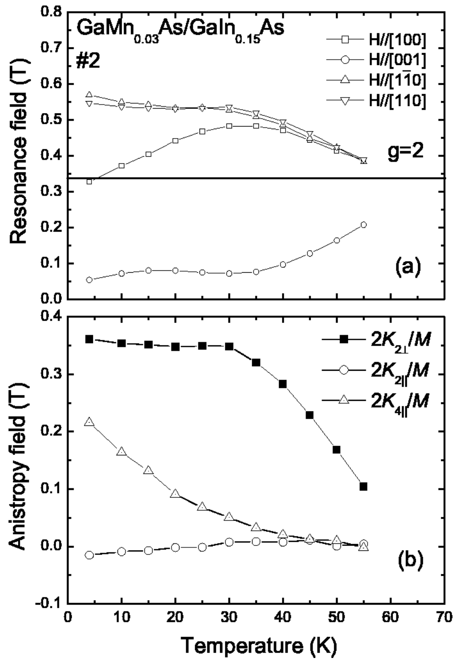

FIG. 9. (a) Temperature dependence of FMR fields observed for four high-symmetry field orientations of **H** for $Ga_{0.97}Mn_{0.03}As/Ga_{0.85}In_{0.15}As$ (sample No. 2). (b) Magnetic anisotropy fields $2K_{2\perp}/M$, $2K_{2\parallel}/M$, and $2K_{4\parallel}/M$ as a function of temperature for the same sample. The solid lines are guides for the eye.

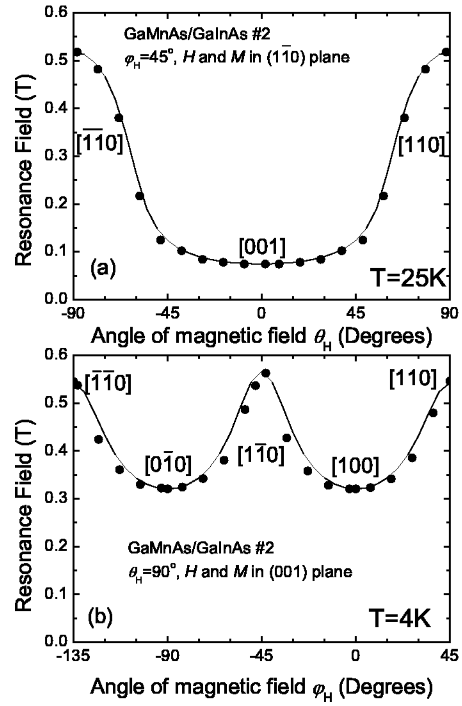

FIG. 10. Angular dependence of FMR fields for the $Ga_{0.97}Mn_{0.03}As/Ga_{0.85}In_{0.15}As$ (sample No. 2), for (a) **H** in the $(1\bar{1}0)$ plane (geometry A) and (b) for **H** in the (001) plane (geometry B). The solid curves in figure represent the positions of H_R calculated theoretically using the full Eqs. (2a) and (2b) for the two geometries, respectively.

We calculate the temperature dependence of the anisotropy fields $2K_{2\perp}/M$, $2K_{4\parallel}/M$, and $2K_{2\parallel}/M$ for the GaMnAs/InMnAs sample using Eqs. (3a)–(3d) and the values of M measured by SQUID, as had been done for GaMnAs/GaAs. The results are plotted in Fig. 9(b). Similar to GaMnAs/GaAs, the magnitudes of all anisotropy fields decrease as the temperature increases, approaching zero close to the Curie temperature.

In Fig. 10 we show the full angular dependences of the resonance field H_R for the GaMnAs/GaInAs film measured in geometry A (top panel) and geometry B (bottom) at a fixed temperature. The solid lines are theoretical curves calculated using the anisotropy fields shown in Fig. 9 by assuming $g=2.0$ in the general equations given in Eq. (2). As in the case of GaMnAs/GaAs, the agreement with experiment is excellent, supporting the accuracy of the model and of the values of the anisotropy fields shown in Fig. 9.

Note in the top panel of Fig. 10 that, when the field **H** is tilted away from the hard ([110]) axis, the direction of **M** immediately begins to seek the easy orientation, as evidenced by the nonsinusoidal shape of the angular dependence. This effect has already been noted in Fig. 6 for GaMnAs/GaAs, but is much stronger in the present case of GaMnAs/GaInAs. The bottom panels of Fig. 10 shows that in the GaMnAs/GaInAs combination there is also a much stronger fourfold in-pane anisotropy fields $H_{4\parallel}$, and again a very small but unmistakable planar twofold uniaxial anisotropy, that we ascribe to the presence of the $H_{2\parallel}$ field. It is also interesting to note that—as can be inferred from the nonsinusoidal nature of the angular dependence of H_R in Fig. 10(b)—when **M** is in the sample plane, it tends to seek the [100] direction even when that is not the real easy axis of the tetragonally strained material as a whole.

Finally, it is instructive to compare the magnitudes of the anisotropy fields for GaMnAs/GaAs in Fig. 6 (sample No. 1) and GaMnAs/GaInAs in Fig. 10 (sample No. 2). We know from the XRD data that sample No. 1 has a compressive strain $\varepsilon_0=(a_s-a_0)/a_0=-0.00135$, and sample No. 2 has a larger tensile strain of $\varepsilon_0=0.00701$. Since the quantity $H_{2\perp}$ is not only opposite in sign, but is also larger in sample No. 2 than in sample No. 1, this illustrates very nicely that anisotropy fields (and especially $H_{2\perp}$) track the magnitude of the strain in the layers, suggesting that FMR on GaMnAs grown epitaxially on buffers with different lattice constants provides an excellent opportunity for quantitatively controlling the effects of magnetic anisotropy in this material.

V. SUMMARY AND CONCLUSIONS

The measurements of FMR presented in this paper show unambiguously that magnetic anisotropy fields play a decisive role in determining the resonance spectrum of epitaxially grown GaMnAs. Since the crystal structure of epitaxial GaMnAs is slightly tetragonal due to the distortion of its relaxed cubic structure by lattice mismatch with the substrate, it is expected that the magnetic anisotropy of this material will be dominated by uniaxial anisotropy. In samples examined in this paper we have observed uniaxial anisotropy fields $2K_{2\perp}/M$ as large as 4000 G—and larger values can probably be induced by greater lattice mismatches than those used in growing the present samples. The sign of the $2K_{2\perp}/M$ term is determined by whether the strain in the layer plane is tensile or compressive, as clearly revealed by the positions of FMR observed for GaMnAs/GaAs and GaMnAs/GaInAs, respectively.

The cubic (fourth-order) anisotropy fields are also very large in GaMnAs (of the order of 2000 G), as evidenced by the angular variation of FMR observed when the orientation of **H** is varied in the basal (001) plane. Finally, these experiments also reveal that there is a small but finite in-plane *uniaxial* anisotropy field $K_{2\parallel}$, signaling a slight uniaxial distortion of GaMnAs in the basal plane itself, that we ascribe to the physical difference between the [110] and $[1\bar{1}0]$ directions of the zinc blende structure on which GaMnAs is grown. The agreement between the experimentally observed angular dependence of the FMR field and the calculated values of H_R obtained using the same values of the anisotropy fields for all field orientations serves as strong evidence that the model used for epitaxial GaMnAs (tetragonal symmetry induced by lattice mismatch, with a small uniaxial distortion of the basal plane along the [110] direction) is accurate.

Our work has revealed that the process of low-temperature annealing, which is known to produce an increase in the Curie temperature, also results in a very significant modification of FMR. Although the data presented is not exhaustive, two prominent aspects emerge from comparison of FMR observed on the same material before and after it was annealed. First, the changes induced by annealing (such as an increase in the Curie temperature) are accompanied by a large change in the magnitude of the anisotropy fields (see Fig. 7). And second, annealing also has resulted in a dramatic narrowing of ΔH_{pp}, as seen in Fig. 8. These results suggest that annealing can be useful in future FMR studies, allowing one to vary the magnetic properties within the same sample for purposes of comparison and correlation.

Finally we wish to point to the clear presence of spin wave resonances that accompany FMR, as seen in Fig. 3. Although a discussion of this phenomenon lies outside the scope of the present paper, it illustrates the richness of the physics related to dynamic magnetization effects that can be investigated in GaMnAs (and presumably other III-Mn-V ferromagnetic semiconductors) by FMR techniques.

ACKNOWLEDGMENTS

The authors are grateful to B. Janko (Notre Dame) and G. Zarand (Harvard) for illuminating discussions. This work was supported by the DARPA/SpinS Program through the Office of Naval Research and by NSF Grant No. DMR02-10519.

*Electronic address: furdyna.1@nd.edu

[1] H. Ohno, Science (Washington, DC, U.S.) **281**, 951 (1998).

[2] J. K. Furdyna, P. Schiffer, Y. Sasaki, S. J. Potashnik, and X. Y. Liu, in *Optical Properties of Semiconductor Nanostructures*, NATO Science Series, Vol. 81, edited by M. L. Sadowski, M. Potemski, and M. Grynberg (Kluwer, Dordrecht, 2000), p. 211–224.

[3] For a detailed review see H. Ohno, J. Magn. Magn. Mater. **200**, 110 (1999).

[4] See, e.g., T. Dietl, H. Ohno, F. Matsukura, J. Cibert, and D. Ferrand, Science (Washington, DC, U.S.) **287**, 1019 (2000).

[5] A. Oiwa, S. Katsumoto, A. Endo, M. Hirasawa, Y. Iye, F. Matsukura, A. Shen, Y. Sugawara, and H. Ohno, Physica B **249**, 775 (1998).

[6] T. Hayashi, Y. Hashimoto, S. Katsumoto, and Y. Iye, Appl. Phys. Lett. **78**, 1691 (2001).

[7] S. J. Potashnik, K. C. Ku, S. H. Chun, J. J. Berry, N. Samarth, and P. Schiffer, Appl. Phys. Lett. **79**, 1495 (2001).

[8] A. Shen, A. Oiwa, A. Endo, S. Katsumoto, Y. Iye, H. Ohno, F. Matsukura, Y. Sugawara, N. Akiba, and T. Kuroiwa, J. Cryst. Growth **175/176**, 1069 (1997).

[9] J. König, J. Schliemann, T. Jungwirth, and A. H. MacDonald, in *Electronic Structure and Magnetism of Complex Materials*, edited by D. J. Singh and D. A. Papaconstantopoulos (Springer Verlag, Berlin, 2002).

[10] G. Schmidt and L. Molenkamp, in *Semiconductor Spintronics and Quantum Computing*, edited by A. D. Awschalom, D. Loss, and N. Samarth (Springer Verlag, Berlin, 2002).

[11] D. Chiba, N. Akiba, F. Matsukura, Y. Ohno, and H. Ohno, Appl. Phys. Lett. **77**, 1873 (2000); M. Tanaka and Y. Higo, Phys. Rev. Lett. **87**, 026602 (2001); S. H. Chun, S. J. Potashnik, K. C. Ku, P. Schiffer, and N. Samarth, Phys. Rev. B **66**, 100408 (2002).

[12] H. X. Tang, R. K. Kawakami, D. D. Awschalom, and M. L. Roukes, Phys. Rev. Lett. **90**, 107201 (2003).

[13] M. Farle, Rep. Prog. Phys. **61**, 755 (1998).

[14] Y. Sasaki, X. Liu, J. K. Furdyna, M. Palczewska, J. Szczytko, and A. Twardowski, J. Appl. Phys. **91**, 7484 (2002).

[15] Note that the linear dependence of the $Ga_{1-x}Mn_xAs$ lattice constant on x given in Ref. 3 yields 0.598 nm when extrapolated to $x=1.00$. A careful study of this issue has been recently made by G. Schott, W. Faschinger, and L. W. Molenkamp, Appl. Phys. Lett. **79**, 1807 (2001).

[16] P. E. Wigen, Phys. Rev. **133**, A1557 (1964).

[17] Y. Zhai, Y. X. Xu, J. G. Long, Y. B. Xu, M. Lu, Z. H. Lu, H. R. Zhai, and J. A. C. Bland, J. Appl. Phys. **89**, 7290 (2001).

[18] S. V. Vonsovskii, *Ferromagnetic Resonance* (Pergamon, Paris, 1966).

[19] J. J. Krebs, B. T. Jonker, and G. A. Prinz, J. Appl. Phys. **61**, 2596 (1987).

[20] K. M. Yu, W. Walukiewicz, T. Wojtowicz, I. Kuryliszyn, X. Liu, Y. Sasaki, and J. K. Furdyna, Phys. Rev. B **65**, 201303 (2002).